Inorganic Chemistry

pubs.acs.org/IC

Article

Influence of the Increasing Number of Organic Radicals on the Structural, Magnetic, and Electrochemical Properties of the Copper(II)−Dioxothiadiazole Family of Complexes

Mirosław Arczyński* and Dawid Pinkowicz*

Cite This: *Inorg. Chem.* 2020, 59, 13489−13501

Read Online

ACCESS | Metrics & More | Article Recommendations | Supporting Information

ABSTRACT: The preparation, structures, and electrochemical and magnetic properties supported by density functional theory (DFT) calculations of three new copper(II) compounds with [1,2,5]thiadiazolo[3,4-*f*][1,10]phenanthroline 1,1-dioxide (td) and its radical anion ($td^{\cdot-}$) are reported: {[Cu^{II}Cl(td)](μ-Cl)$_2$[Cu^{II}Cl-(td)]} (**1**), which incorporates only neutral td ligands; [Cu^{II}Cl($td^{\cdot-}$)(td)]·2MeCN (**2**), which comprises one neutral td and one radical $td^{\cdot-}$; and PPN[Cu^{II}Cl($td^{\cdot-}$)$_2$]·2DMA (**3**), where Cu^{II} ions are coordinated by two radical anions $td^{\cdot-}$ (DMA, dimethylacetamide; PPN^+, the bis(triphenylphosphine)iminium cation). All three compounds show interesting paramagnetic behavior with low-temperature features indicating significant antiferromagnetic coupling. The magnetic properties of **1** are dominated by $Cu^{II}\cdots Cu^{II}$ interactions (J_{CuCu}) mediated through the Cl^- bridges, while the magnetic properties of **2** and **3** are governed mainly by the $td^{\cdot-}\cdots td^{\cdot-}$ (J_{tdtd}) and Cu^{II}–$td^{\cdot-}$ (J_{Cutd}) exchange interactions. The structure of **2** features only two major magnetic coupling pathways enabling the fitting of experimental data with J_{tdtd} = −36.0(5) cm^{-1} and J_{Cutd} = −12.6(2) cm^{-1} only. Compound **3** exhibits a complex network of magnetic contacts. Attempt to approximate its magnetic behavior using only a local magnetic contacts model resulted in J_{tdtd} = −5.6(1) cm^{-1} and two J_{Cutd} constants, −12.4(2) and −22.6(4) cm^{-1}. The experimental fitting is critically compared with the results of broken symmetry density functional theory (BS DFT) calculations for inter- and intramolecular contacts. More consistent results were obtained with the M06 functional as opposed to popular B3LYP, which encountered problems reproducing some of the experimental intermolecular exchange interactions. Electrochemical measurements of **2** and **3** in MeCN showed three reversible nearly overlapping redox peaks appearing in a narrow potential range of −600 to −100 mV vs Fc/Fc^+. Small differences between the redox events suggest that such compounds may be good candidates for new switchable materials, where the electron transfer between the metal and the ligand center is triggered by temperature, pressure, or light (valence tautomerism).

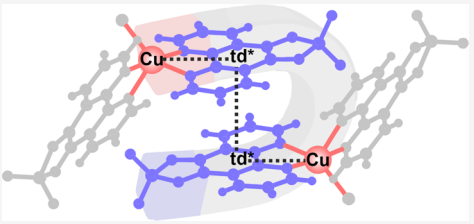

INTRODUCTION

Over the past two decades, the molecular magnetism community has advanced from studying the basic rules governing the magnetic coupling in paramagnetic molecules toward the design and synthesis of multifunctional molecular materials.[1] However, understanding the mechanism of magnetic interactions in molecular magnets is still a crucial task, especially in view of the recent trends in designing weakly coupled molecular qubit arrays.[2]

Organic radical ligands very often show moderate-to-strong magnetic interactions with metal ions[3] due to the large spin density at the donor atoms, which in combination with their redox noninnocence[4−6] and chemical tunability results in fascinating magnetic behaviors.[5] On top of that, radicals are well known for their catalytic activity and biological importance.[7−11] Notably, molecular magnetism and catalysis share a library of organic radicals.[3,7] It is thus crucial to develop a chemical and theoretical understanding of new organic radicals in order to increase the number of nonmetal paramagnetic building blocks for the synthesis of functional and multifunctional molecular materials.[5] Among many different functionalities of radical-based magnetic compounds, the following seem to be the most popular: electronic conductivity,[12−14] long-range magnetic ordering,[15−19] valence tautomerism,[6,20−22] photomagnetism,[20,23−28] luminescence,[29−32] and single molecule and single chain magnet behavior (SMM and SCM).[3,33−36]

Even though the library of organic radicals is enormous,[3,20,37−40] only a few classes dominate the field of molecular magnetism, and these are verdazyls,[41,42] nitronyl nitroxides,[43,44] semiquinones,[45,46] and TTF, TCNE, and TCNQ derivatives.[47−52] The popularity of these four groups is dictated by their stability, chemical tunability, coordination abilities promoting strong magnetic interactions, and electro-

Received: June 27, 2020
Published: September 10, 2020

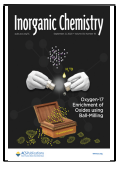

https://dx.doi.org/10.1021/acs.inorgchem.0c01904
Inorg. Chem. 2020, 59, 13489−13501

chemical properties providing electron transfer and enabling various types of switching properties.

Herein, we focus on the properties of [1,2,5]thiadiazolo[3,4-*f*][1,10]phenanthroline 1,1-dioxide (td), which belongs to the group of dioxothiadiazole-based electroactive molecules,[53−60] and the influence of its valence state on the outcome of its reaction with Cu^{II}. The td molecule shows three features important from the point of view of the design of new magnetic materials: (i) it can be easily reduced to an air-stable radical anion (S = 1/2), (ii) it shows strong coordination abilities via the 1,10-phenanthroline backbone, and (iii) its rigid nonflat geometry favors specific supramolecular arrangements involving anion−π-type contacts. According to DFT calculations, the unpaired electron of the $td^{\cdot-}$ radical anion is mostly delocalized over the thiadiazole ring and partially localized on the nitrogen atoms of the 1,10-phenanthroline backbone, suggesting the possibility of medium-to-strong metal−radical magnetic interactions in the case of its coordination to paramagnetic metal centers.[54,56] In this context, we decided to investigate the magnetic exchange interactions between the paramagnetic transition-metal center and the $td^{\cdot-}$ radical anions by using a combined experimental and theoretical approach. This is the first report where the dioxothiadiazole-type radical ligand is coordinated to a paramagnetic transition-metal center. The choice of Cu^{II} (S = 1/2) is dictated by the fact that complexes with this particular metal ion are a good model systems for the in-depth investigation of the magnetic interactions in molecular materials including DFT methods.[61−65] The main advantage of Cu^{II} is its simplicity: only one unpaired electron, the lack of the first-order orbital momentum, and the absence of zero-field splitting effects.[66]

In this article, we present the experimental and theoretical (broken-symmetry DFT) survey of the structural, electrochemical, and magnetic properties of three new Cu^{II}−td complexes with an increasing number of coordinated $td^{\cdot-}$ radical anions: {[Cu^{II}Cl(td)](μ-Cl)$_2$[Cu^{II}Cl(td)]} (**1**) coordinated solely by neutral td ligands (no radicals), [Cu^{II}Cl($td^{\cdot-}$)(td)]·2MeCN (**2**) (MeCN, acetonitrile) with one neutral and one reduced td (one radical anion), and PPN[Cu^{II}Cl($td^{\cdot-}$)$_2$]·2DMA (**3**) (DMA, dimethylacetamide) with two radical $td^{\cdot-}$ anions. Compound **1** was analyzed by assuming one type of exchange interaction through the Cu^{II}−Cl−Cu^{II} bridges which proved to be weakly antiferromagnetic, while compounds **2** and **3** reveal complex magnetic behavior dominated by antiferromagnetic interactions involving Cu^{II} metal centers (S = 1/2) and $td^{\cdot-}$ radicals (S = 1/2) via Cu^{II}−Cl···Cu^{II}, Cu^{II}−$td^{\cdot-}$, and $td^{\cdot-}$···$td^{\cdot-}$ intermolecular contacts (···) and coordination bonds, respectively (−). Electrochemical properties (cyclic voltammetry, CV) were also investigated for complexes **2** and **3** in order to confirm the potential of Cu^{II}−td pairs for the construction of switchable molecular materials.

RESULTS AND DISCUSSION

Synthesis. Single crystals of **1** are obtained by the slow diffusion of MeCN solutions of $Cu^{II}Cl_2·2H_2O$ and td. Direct mixing leads to a fast precipitation of a shimmering crystalline powder. Both methods result in pure samples of **1**.

In our first approaches to the synthesis of compound **2**, hot MeCN solutions of Cu^{I}Cl and td were mixed, and the reaction mixture was left to crystallize under ambient conditions. This method, however, leads to impure samples. To obtain pure compound **2**, a hot MeCN mixture of Cu^{I}Cl and td needs to be quickly filtered and the hot filtrate is left for crystallization at 60 °C. The reaction takes advantage of the redox potentials of td and Cu^{I}Cl in hot MeCN: Cu^{I} is oxidized to Cu^{II} by one of the td ligands with its concomitant reduction to radical form $td^{\cdot-}$. This is consistent with the CV results presented below.

The most straightforward way to obtain compound **3** is through the slow vapor diffusion of diethyl ether into the DMA solution of radical anion salt PPN$td^{\cdot-}$ and $Cu^{II}Cl_2·2H_2O$. This method yields relatively large crystals of **3**.

The purity of all products was carefully verified by elemental analysis and powder X-ray diffraction (PXRD) of the samples immersed in the mother solution (Figure S1 in the Supporting Information). The Le Bail refinement of the unit cell parameters (Table S1 in the Supporting Information) against the room-temperature experimental PXRD patterns using the scXRD unit cell parameters as the starting values (color solid lines and bars in Figure S1) was done to confirm that the slight differences between the room-temperature PXRD and the simulated low-temperature scXRD patterns are solely due to the thermal expansion effects. Indeed, the positions of the diffraction peaks after Le Bail refinement (bars) are in perfect agreement with the experimental room-temperature PXRDs. The Le Bail refined unit cell parameters are presented in Table S2 in the Supporting Information.

Structural Analysis. Reported compounds **1**−**3** crystallize in centrosymmetric space group $P\bar{1}$. Details of the structure refinement can be found in Table S1 (in the SI). The asymmetric units are presented in Figure 1. The valence state assignment of the td ligands in **1**−**3** is based on the number of anions and cations in the crystal structures and the careful analysis of the td bond lengths (Table 1). The reduction of td to a radical anion leads to a strong shortening of the C−C ("CC") bond of the dioxothiadiazole ring by ca. 0.06 Å (based on the observations of Awaga et al.[53−55]). Most importantly, this particular structural change occurs regardless of the coordination mode of the ligand.

Crystal Structure of 1. **1** forms dinuclear molecules {[CuCl(td)](μ-Cl)$_2$[CuCl(td)]} with two chloride anions bridging two Cu^{II} metal centers. The asymmetric unit (Figure 1a) comprises only half of the molecule, with the second half being reproduced by the inversion center. Each Cu^{II} is coordinated by a neutral td ligand and three chloride anions (one terminal and two bridging), resulting in a distorted square-pyramidal geometry. (Continuous shape measure (CShM) analysis leads to the following shape parameters: 1.175 for square pyramid SPY-5, 2.089 for vacant octahedron vOC-5, and 4.465 for trigonal bipyramid TBPY-5; see Table S3 in the Supporting Information.) The analysis of the Cu−Cl (2.240(3), 2.273(3), and 2.651(3) Å) and Cu−N (2.053(10) and 2.046(11) Å) bond lengths reveals strong Jahn−Teller distortion along the Cu1−Cl2 bond of 2.651(3) Å. (See also Table S4 in the Supporting Information). The td ligands in **1** are neutral, which is supported by the dioxothiadiazole ring C−C (CC) bond length of 1.503(17) Å, and are arranged in such a way that the oxygen atoms of one ligand are directed toward the electron-deficient CC bond of the dioxothiadiazole group of the adjacent molecule (Figure 2), with a O···CC distance of ca. 2.93 Å. Additional supramolecular contacts involving the dioxothiadiazole CC bonds are formed by the terminal Cl^- ligands (Cl···CC of ca. 3.01 Å).

Crystal Structure of 2. The asymmetric unit of **2** (Figure 1b) consists of a mononuclear complex [CuCl($td^{\cdot-}$)(td)] and two crystallization molecules of acetonitrile (one is slightly

https://dx.doi.org/10.1021/acs.inorgchem.0c01904
Inorg. Chem. 2020, 59, 13489−13501

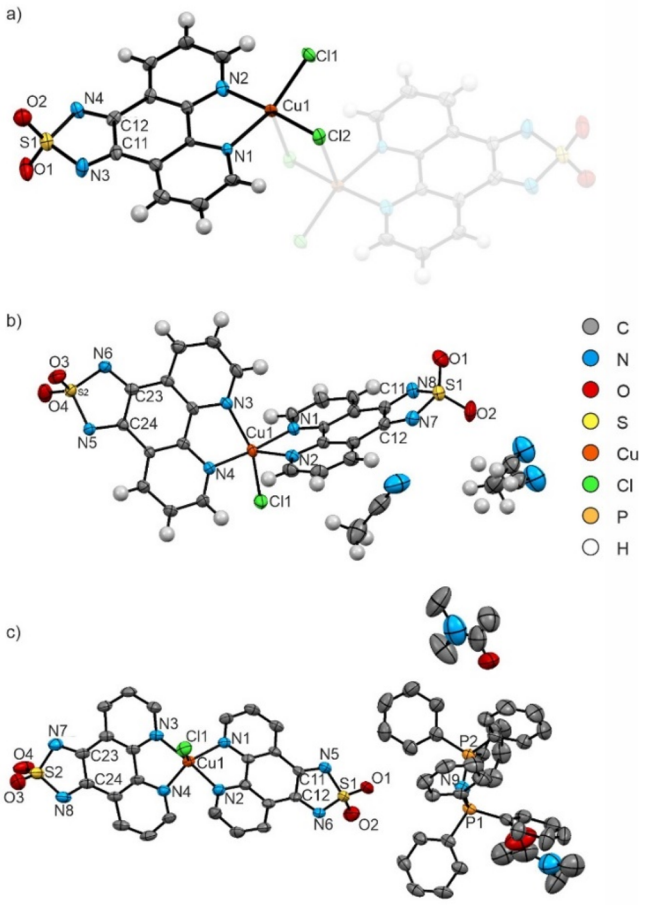

Figure 1. Structural diagrams of the asymmetric units of (a) **1**, (b) **2**, and (c) **3** with ellipsoids at the 70% probability level. Colors: Cu, orange; Cl, green; S, bright yellow; P, dark yellow; O, red; N, blue; C, gray; and H, white or ommited. (The same colors apply to all structural diagrams.) Note that (a) also illustrates a symmetry-dependent part (dimmed) to better visualize the dinuclear character of **1**.

disordered). Cu^{II} metal centers are coordinated by one chloride (Cu−Cl: 2.2872(6) Å), two nitrogen atoms of the neutral td (Cu−N: 1.9884(17) and 2.1851(18) Å), and two nitrogen atoms of radical anion $td^{\cdot-}$ (Cu−N: 2.0620(18) and 1.9893(17) Å), resulting in a penta-coordinate geometry somewhere between a square pyramid and a trigonal bipyramid (CShM analysis parameters are 2.599 for SPY-5, 3.106 for vOC-5 and 2.883 for TBPY-5 see also Table S3 in the Supporting Information for CShM parameters and Table S4 in the Supporting Information for selected bond lengths). The analysis of the dioxothiadiazole ring geometry supports the proposed valence state assignment: one neutral and one radical ligand coordinated to Cu^{II}. The CC bond length in the radical anion is 1.453(3) Å, while the corresponding one in the neutral ligand is 1.513(3) Å (Figure 3 and Table 1). The $[CuCl(td^{\cdot-})(td)]$ molecules in compound **2** form supramolecular pairs with $\pi-\pi$ contacts between the radical ligands ($td^{\cdot-}\cdots td^{\cdot-}$ ca. 3.5 Å) which are strengthened by intramolecular σ-donor−π-acceptor interactions[67,68] between the $>SO_2$ group of the radical $td^{\cdot-}$ and the central C_6 ring of the neutral td (Figure 3b). The supramolecular pairs are further "expanded" into quasi-chains by weaker alternating Cu^{II}−Cl···Cu^{II} contacts (Cu···Cu ca. 4.5 Å) (Figure 3b). It is noteworthy that the propagation direction of the quasi-chains coincides with the *a* crystallographic direction, which shows unusually large thermal elongation. The neutral ligands are pointing perpendicular to the direction of chain propagation engaging in interchain O··· CC contacts with $>SO_2$ groups of the radical $td^{\cdot-}$ ligands. There is no structural indication of $\pi-\pi$ contacts involving neutral td ligands only.

Crystal Structure of ***3***. The asymmetric unit of **3** contains a PPN^+ cation, a $[CuCl(td^{\cdot-})_2]^-$ complex anion, and two dimethylacetamide crystallization solvent molecules (Figure 1c). Each of the $td^{\cdot-}$ ligands is in the radical anion form (dioxothiadiazole C−C bonds of 1.450(4) Å and 1.452(4) Å, respectively; see Table 1 for details), so the presence of the PPN^+ cation in the crystal structure is necessary to balance the negative charge of the coordinated chloride. Cu^{II} adopts a distorted trigonal bipyramidal geometry (CShM analysis parameters are 4.579 for SPY-5, 1.091 for TBPY-5, and 6.399 for vOC-5; see also Table S3 in the Supporting Information for CShM parameters and Table S4 for selected bond lengths). It is coordinated by four nitrogen atoms of the $td^{\cdot-}$ radical anions (Cu−N: 2.121(3), 1,982(3), 1.999(3), and 2.079(3) Å) and one chloride (Cu−Cl: 2.302(1) Å).

Every two $[CuCl(td^{\cdot-})_2]^-$ molecules in **3** form a supramolecular pair (Figure 4a) very similar to those in compound **2** with the corresponding $\pi-\pi$ contacts between the $td^{\cdot-}$ radicals of ca. 3.4 Å and the σ-donor−π-acceptor type interactions between the $>SO_2$ group of one radical $td^{\cdot-}$ and the central C_6 ring of the other one. This highlights the extraordinary stability of the supramolecular pairs in both **2** and **3** and the strength of the relevant molecular contacts despite the anionic character of the $[CuCl(td^{\cdot-})_2]^-$ moieties in **3**. The PPN^+ cations and the pairs of $[CuCl(td^{\cdot-})_2]^-$ anions form supramolecular layers (Figure 4b,c) with the crystallization solvent molecules occupying the empty spaces formed by the PPN^+ cations. The anionic layers are stabilized by local weak $\pi-\pi$ contacts between the $td^{\cdot-}\cdots td^{\cdot-}$ ligands of the aforementioned supramolecular pairs. (The shortest centroid-to-centroid distances between the radicals are 6.840 and 6.225 Å.)

Magnetic Properties. *Magnetic Properties of Compound* ***1***. **1** shows paramagnetic behavior with a signature of weak antiferromagnetic coupling. The $\chi T(T)$ dependence (Figure 5a) remains constant at 0.79 cm^3 K mol^{-1} in the 300−40 K range and then starts to decrease to reach 0.32 cm^3 K mol^{-1} at 1.8 K.

The high-temperature χT value is in agreement with that expected for two noninteracting Cu^{II} ions assuming g_{Cu} = 2.05 and S = 1/2. The observed $\chi T(T)$ decrease below 40 K is due to weak antiferromagnetic interactions between the chloride-bridged Cu^{II} ions. The field dependence of the molar magnetization shows a gradual increase with an inflection at around 1.2 T and slow flattening above 6 T reaching 1.9μ_B at 7 T. This is very close to the expected 2.06μ_B assuming two weakly interacting Cu^{II} centers with g_{Cu} = 2.05 and S = 1/2.

According to the scXRD studies, **1** is a dinuclear molecule with Cl^- acting as molecular bridges. Therefore, in order to fit its magnetic properties (PHI software;[68] green solid lines in Figure 5a), the following Hamiltonian was used assuming a single magnetic interaction pathway between the Cu^{II} centers (Figure 5b):

$$\hat{H}_1 = \mu_B g_{Cu} B S_{Cu1} + \mu_B g_{Cu} B S_{Cu2} - 2J_{CuCu} S_{Cu1} S_{Cu2} \quad (1)$$

https://dx.doi.org/10.1021/acs.inorgchem.0c01904
Inorg. Chem. 2020, 59, 13489−13501

Table 1. Comparison of the Bond Lengths (Å) within the Dioxothiadiazole Rings[a] of the td Ligands in 1−3 and in Selected Compounds Reported in Reference 54

		S=O	S-N	C=N	C-C
Neutral form	1	1.419(11)	1.683(11)	1.273(16)	1.503(17)
		1.420(10)	1.703(10)	1.287(16)	
	2	1.423(2)	1.695(2)	1.280(3)	1.513(3)
		1.419(2)	1.699(2)	1.283(3)	
	Average in 1 and 2	**1.420**	**1.695**	**1.281**	**1.508**
	From ref. [54]	**1.427**	**1.687**	**1.289**	**1.508**
Radical anion form	2	1.444(2)	1.652(2)	1.329(3)	1.453(3)
		1.436(2)	1.650(2)	1.328(3)	
	3	1.439(3)	1.662(3)	1.330(4)	1.450(4)
		1.433(3)	1.643(3)	1.325(4)	
		1.431(3)	1.660(3)	1.321(4)	1.452(4)
		1.434(3)	1.664(3)	1.321(4)	
	Average in 2 and 3	**1.436**	**1.655**	**1.326**	**1.452**
	From ref. [54]	**1.442**	**1.641**	**1.340**	**1.434**

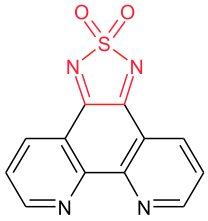

[a]See the red part of the structural formula in the last column.

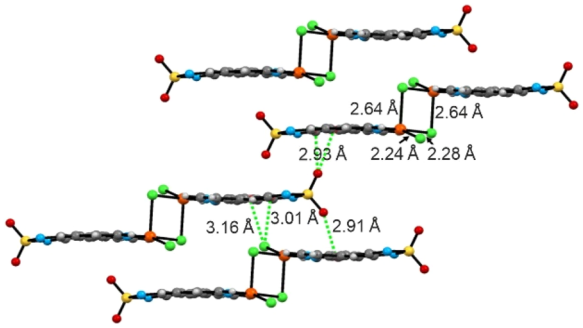

Figure 2. Structural diagram presenting Cu−Cl bond lengths and intermolecular contacts in compound **1.**

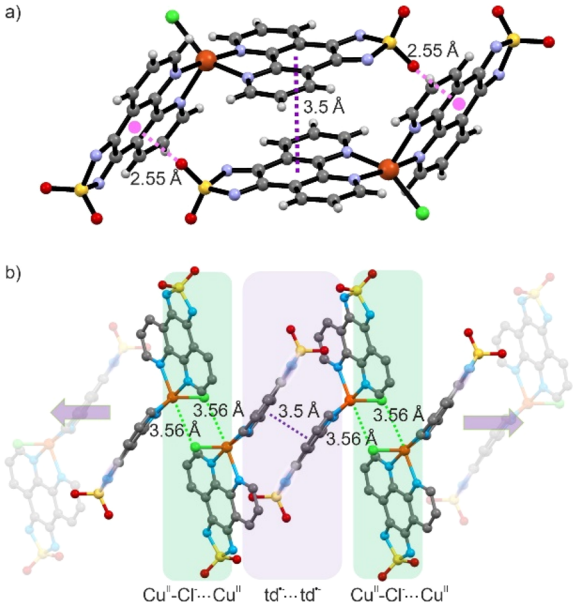

Figure 3. Structural diagrams for **2** demonstrating the formation of supramolecular pairs based on td$^{\cdot-}$···td$^{\cdot-}$ and td$^{\cdot-}$···td interactions (a) which extend further into a supramolecular chain formed by Cu^{II}−Cl···Cu^{II} contacts (b). Violet arrows show the direction of the supramolecular chain propagation which is parallel to the crystallographic *a* direction. Note that the peripheral translucent molecules are the repetition of the main fragments.

(g_{Cu} is the average isotropic *g* parameter of the two Cu^{II} ions in the molecule, J_{CuCu} is the isotropic exchange coupling constant, μ_B is the Bohr magneton, and *B* is the magnetic field). Both magnetization and magnetic susceptibility data were fitted simultaneously. The best-fit parameters are summarized in Table 2. Both $\chi T(T)$ and $M(H)$ fits match the experimental data well (Figure 6a).

Magnetic Properties of Compound ***2****.* **2** also exhibits paramagnetic behavior with a very clear indication of moderate antiferromagnetic coupling as the $\chi T(T)$ value decreases from 0.72 cm^3 K mol^{-1} (close to 0.75 cm^3 K mol^{-1} expected for two noninteracting $S = 1/2$ moieties (Cu^{II} and a radical td$^{\cdot-}$) to almost zero at 2.0 K (Figure 6a). The $M(H)$ curve (Figure 6a inset) recorded at 1.8 K in the 0−4.5 T range shows only a small increase in the magnetization, reaching 0.2 μ_B at 4.5 T without saturation, which is expected for two $S = 1/2$ moieties coupled antiferromagnetically (assuming moderate interactions).

At first glance, compound **2** is a two-spin system comprising a single Cu^{II} center and one radical td$^{\cdot-}$. Hence, one would expect that the observed magnetic behavior with a basically nonmagnetic ground state is due to the antiferromagnetic interactions between the Cu^{II} and the radical (J_{Cutd}). However, a careful examination of the crystal structure indicates an intermolecular contact between the td$^{\cdot-}$ ligands within the supramolecular pairs of [Cu^{II}Cl(td$^{\cdot-}$)(td)] molecules. Such contacts have been shown to be very efficient pathways for moderate and strong magnetic interactions.[54] Therefore, they must be included in the fitting of the magnetic properties as an

https://dx.doi.org/10.1021/acs.inorgchem.0c01904
Inorg. Chem. 2020, 59, 13489−13501

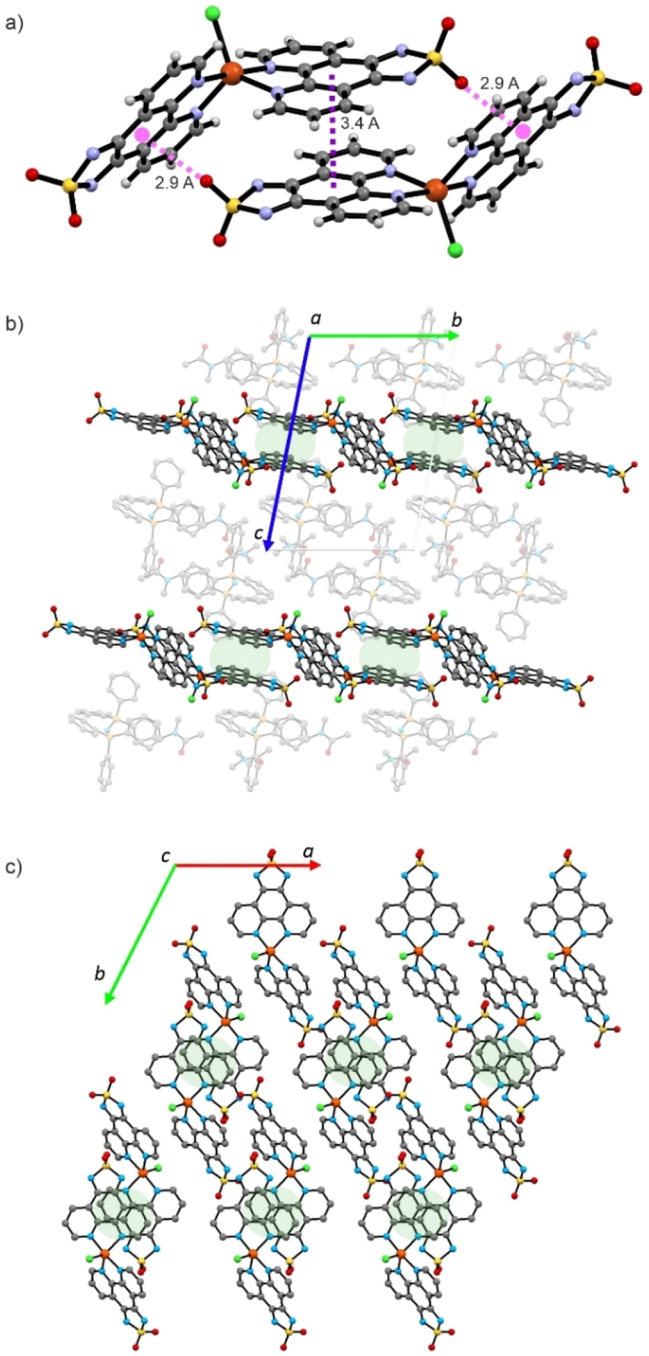

Figure 4. Structural diagrams for **3** demonstrating the formation of supramolecular pairs based on $td^{\cdot-}\cdots td^{\cdot-}$ interactions (a) and packing diagrams showing the alternating layered arrangement of the PPN^+ cations and $[CuCl(td^{\cdot-})_2]^-$ anions in compound **3** (b) and a single anionic layer perpendicular to the *c* crystallographic direction (c). The cationic layers in (b) are rendered partially transparent for clarity. The $\pi-\pi$ pairs of $[CuCl(td^{\cdot-})_2]^-$ anions are highlighted using translucent green ellipses.

additional antiferromagnetic pathway (J_{tdtd}) to reproduce the experimental curves correctly (Figure 6b).

Other molecular contacts such as the aforementioned Cu^{II}–$Cl\cdots Cu^{II}$ contacts (see the crystal structure description) are treated within the mean field model as *zJ* (as implemented in the PHI software).[69] The magnetic properties were successfully fitted (solid red lines in Figure 6a) using the following Hamiltonian with two types of antiferromagnetic interactions

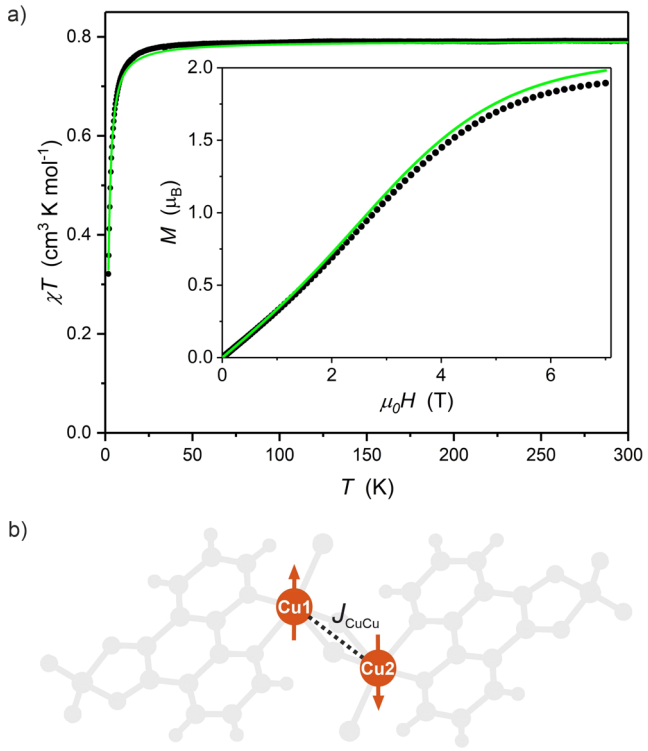

Figure 5. (a) Temperature dependence of the molar magnetic susceptibility and temperature product $\chi T(T)$ recorded for a 0.1 T magnetic field and (inset) the field dependence of the molar magnetization $M(H)$ recorded at 2.0 K for compound **1**. The solid green lines represent the best fit to the experimental data (black points) assuming magnetically isolated molecules with only one type of magnetic interaction as depicted in (b).

Table 2. Best-Fit Parameters Obtained by Fitting the Magnetic Properties of 1–3 Using Equations 1–3

	1 (eq 1)	**2** (eq 2) including *zJ*	**3** (eq 3) including *zJ*
g_{Cu}	2.06 (5)	2.15 (5)	2.15 (5)
J_{CuCu}/cm^{-1}	−1.2 (1)		
J_{Cutd}/cm^{-1}		−12.6 (2)	−22.6 (4)
			−12.4 (2)
J_{tdtd}/cm^{-1}		−36.0 (5)	−5.6 (1)
zJ/cm^{-1}		−1.9 (2)	−0.6 (1)
g_{td} (fixed)		2.00	2.00

within a pair of $[CuCl(td^{\cdot-})(td)]$ molecules (four $S = 1/2$ spin centers, arranged as depicted in Figure 6b)

$$\hat{H}_2 = \mu_B g_{Cu} B S_{Cu1} + \mu_B g_{Cu} B S_{Cu2} + \mu_B g_{td} B S_{td1} + \mu_B g_{td} B S_{td2} - 2J_{Cutd}(S_{Cu1}S_{td1} + S_{Cu2}S_{td2}) - 2J_{tdtd}S_{td1}S_{td2} \quad (2)$$

(g_{Cu} and g_{td} (fixed) are the average *g* parameters of the Cu^{II} ions and td radicals, respectively, J_{Cutd} is the isotropic exchange coupling constant between Cu^{II} and coordinated radical anion $td^{\cdot-}$, and J_{tdtd} is the coupling constant between the $td^{\cdot-}$ radicals of the neighboring $[CuCl(td^{\cdot-})(td)]$ molecules). Both magnetization and magnetic susceptibility data were fitted simultaneously. The best-fit parameters are summarized in Table 2. Both $\chi T(T)$ and $M(H)$ fits match the experimental data.

Magnetic Properties of Compound ***3***. **3** is also a paramagnet showing a strong deviation from Curie's law due to moderate antiferromagnetic interactions. $\chi T(T)$ decreases from 1.08 cm^3 K mol^{-1} expected for three noninteracting $S =$

https://dx.doi.org/10.1021/acs.inorgchem.0c01904
Inorg. Chem. 2020, 59, 13489−13501

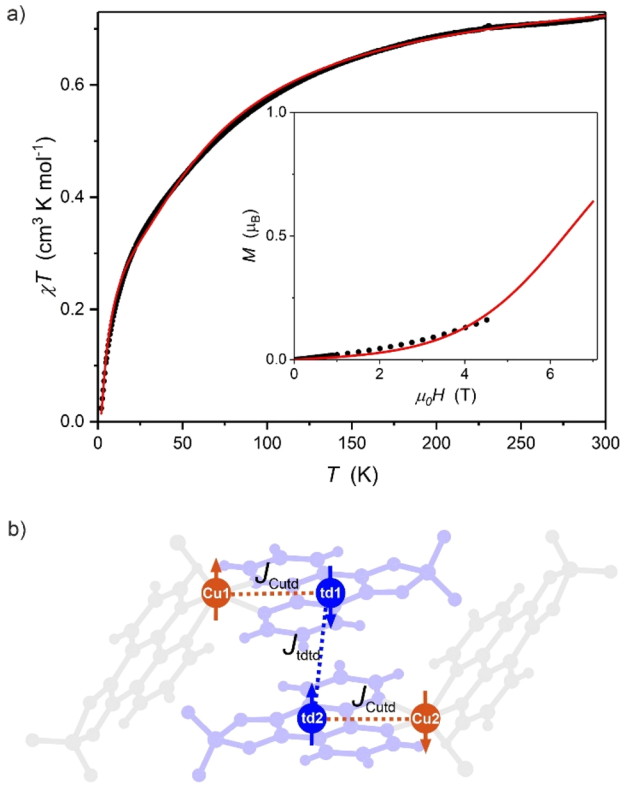

Figure 6. (a) Temperature dependence of the molar magnetic susceptibility and temperature product $\chi T(T)$ recorded at 0.1 T magnetic field and (inset) field dependence of the molar magnetization $M(H)$ recorded at 1.8 K for compound **2**. The solid red lines represent the best fit to the experimental data (black points) assuming two types of strong magnetic interactions: (b) intramolecular J_{Cutd} within each $[CuCl(td^{\cdot-})(td)]$ molecule and intermolecular J_{tdtd} between two neighboring $[CuCl(td^{\cdot-})(td)]$ molecules.

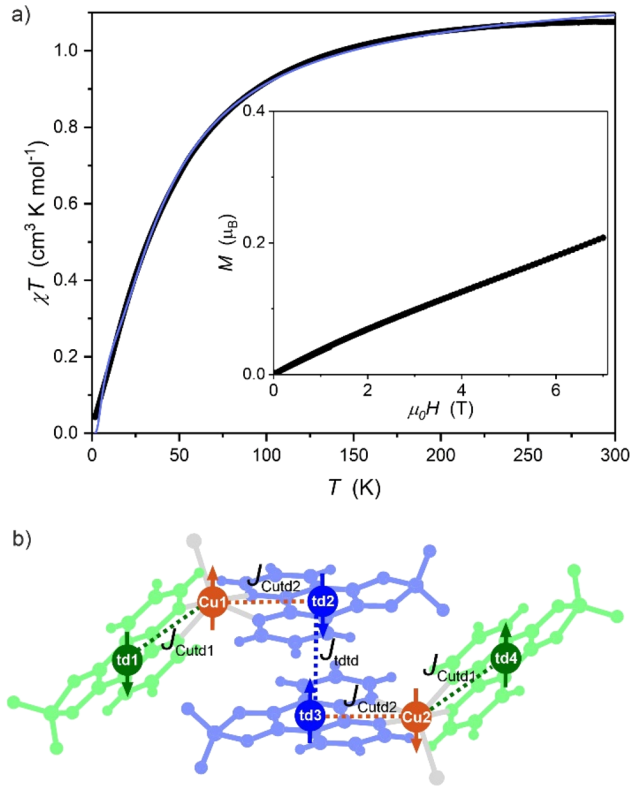

Figure 7. (a) Temperature dependence of the molar magnetic susceptibility and temperature product $\chi T(T)$ recorded at 0.1 T magnetic field and (inset) field dependence of the molar magnetization $M(H)$ recorded at 1.8 K for compound **3**. The blue solid lines represent the best fit to the experimental data (black points) assuming three types of magnetic interactions: (b) intramolecular J_{Cutd1} and J_{Cutd2} within each $[CuCl(td^{\cdot-})(td)]$ molecule and intermolecular J_{tdtd} between $[CuCl(td^{\cdot-})(td)]$ molecules.

1/2 moieties (ca. 1.13 cm^3 K mol^{-1} for one Cu^{II} and two $td^{\cdot-}$radicals) to 0.04 at 2.0 K (Figure 7a). This is well below the expected 0.38 cm^3 K mol^{-1} assuming antiferromagnetic interactions between the central ion and both radical ligands.

The $M(H)$ curve (Figure 7a inset) recorded at 1.8 K in the 0−7 T range shows a gradual increase in the magnetization of up to 0.21 μ_B at 7 T without reaching the saturation value of ca. 1 μ_B expected for three S = 1/2 moieties arranged in a quasi-linear fashion with moderate antiferromagnetic coupling. Moreover, $M(H)$ also deviates from what would be expected for a simple molecule with local antiferromagnetic interactions as in compound **2**.

Both $\chi T(T)$ and $M(H)$ suggest that an additional antiferromagnetic interaction pathway transmitted through the $\pi-\pi$ contacts of the $td^{\cdot-}$ radicals must be included in the analysis of the magnetic behavior of **3**. Moreover, antiferromagnetic interactions with other neighboring molecules through the extensive $\pi-\pi$ contact network in **3** are also possible.

An attempt to fit the $\chi T(T)$ dependence for **3** assuming magnetic interaction pathways for a supramolecular dimer as depicted in Figure 7b (and similar to **2**) did not yield satisfactory agreement with the experimental data below 10 K (blue line in Figure 7a). Assuming this "pair" model, the following Hamiltonian with three types of antiferromagnetic interactions within a pair of $[CuCl(td^{\cdot-})_2]$ molecules (six S = 1/2 spin centers in a linear arrangement as depicted in Figure 7b) was used (including a zJ component):

$$\hat{H}_3 = \mu_B g_{Cu} B S_{Cu1} + \mu_B g_{Cu} B S_{Cu2} + \mu_B g_{td} B S_{td1} + \mu_B g_{td} B S_{td2} + \mu_B g_{td} B S_{td3} + \mu_B g_{td} B S_{td4} - 2J_{Cutd1}(S_{Cu1}S_{td1} + S_{Cu2}S_{td4}) - 2J_{Cutd2}(S_{Cu1}S_{td2} + S_{Cu2}S_{td3}) - 2J_{tdtd}S_{td2}S_{td3} \quad (3)$$

(The meaning of the parameters is analogous to that from eq 2 with indexes in J_{Cutd1} and J_{Cutd2} pointing toward two independent radical ligands.) Only susceptibility data was fitted with eq 3, and the results are gathered in Table 2. These parameters, however, are not as reliable as in **1** and **2** due to the presence of many other moderate magnetic interactions in **3** which could not be taken into account to avoid severe overparameterization. The BS DFT calculations described below support this general conclusion that the magnetic properties of **3** are not dominated by the supramolecular pairs.

BS DFT Calculations. The calculations were carried out with B3LYP and M06 functionals under an unrestricted Kohn−Sham formalism. Several basis sets were tested with the B3LYP functional, but only the results using ma-Def2-SVP (C, H, N, O)/Def2-TZVP (Cu, S, Cl) are presented below. Results for other basis sets are gathered in the Supporting Information (Tables S5−S7 and Comment S1 in the SI). Geometries for the DFT studies were taken from the experimental scXRD structural models.

https://dx.doi.org/10.1021/acs.inorgchem.0c01904
Inorg. Chem. 2020, 59, 13489−13501

Table 3. Results of the BS DFT Calculations for Compound 2[a]

model		1	2	3	4	exp
B3LYP	J_{Cutd}	−14.91		−18.77	−19.12	−12.6 (2)
	J_{tdtd}		−12.53	−1.75		−36.0 (5)
	J_{CuCu}				−0.22	
	zJ					−1.9 (2)
M06	J_{Cutd}	−14.48		−16.31	−22.8	−12.6 (2)
	J_{tdtd}		−33.02	−25.62		−36.0 (5)
	J_{CuCu}				+2.0	
	zJ					−1.9 (2)

[a] J value given in cm^{-1}.

BS DFT Calculations for 1. The J_{CuCu} magnetic interaction in compound **1** calculated with B3LYP and M06 functionals is weakly ferromagnetic (+3.45 cm^{-1} for B3LYP and +5.74 cm^{-1} for M06), which is in direct disagreement with the experiment. However, quantum chemical methods often fail to provide correct estimates of weak magnetic interactions, especially when the coupling constant values are close to zero.[53,55] The total energies and $\langle S^2 \rangle$ expectation values of the triplet and the BS states are presented in Table S8 in the Supporting Information. The spin density illustration of a high-spin-state system calculated with the M06 functional is showed in Figure S3 in the Supporting Information.

BS DFT Calculations for 2. As discussed in previous sections, the crystal structure of compound **2** comprises supramolecular pairs of [CuCl(td$^{\bullet-}$)(td)] complexes (Figures 3a, 6b, and SI S4a). In order to extract magnetic interactions J_{Cutd} and J_{tdtd} within these pairs, the following structural fragments were selected for BS DFT calculations: the [CuCl(td$^{\bullet-}$)(td)] molecule as a two-spin model for the calculation of J_{Cutd} (model 1, Figure S4b), a $\pi-\pi$ pair of td$^{\bullet-}$ radicals as a two-spin model for the calculation of J_{tdtd} (model 2, Figure S4c), a supramolecular $\pi-\pi$ pair of [CuCl(td$^{\bullet-}$)(td)] complexes as a four-spin model for the calculations of J_{Cutd} and J_{tdtd} (model 3, Figure S4d), and a supramolecular Cu−Cl···Cu pair of these complexes as a four-spin model for the calculation of J_{Cutd} and J_{CuCu} (model 4, Figure S4e). Results of the calculations for the four models using B3LYP and M06 functionals are presented in Table 3 and Tables S10−S13 in the Supporting Information.

J_{Cutd} is antiferromagnetic in all models (1, 3, and 4), and the obtained values are in reasonable agreement with the experimental data. Moreover, J_{Cutd} does not seem to be sensitive to the choice of the electron density functional (B3LYP vs M06). The slight difference among models 1, 3, and 4 is most probably caused by the change in the spatial spin density distribution due to the presence or absence of neighboring molecules and coordinated Cu^{II} ions (Figure S5 in the Supporting Information).

The intermolecular J_{tdtd} exchange coupling, on the other hand, depends significantly on the functional used for calculations. Both B3LYP and M06 lead to antiferromagnetic coupling, which is in agreement with the experimental data. However, the B3LYP J_{tdtd} = −12.53 cm^{-1} obtained within model 2 is slightly smaller than the B3LYP J_{Cutd} = −14.91 cm^{-1}, while the corresponding values calculated with M06 are J_{tdtd} = −33.02 cm^{-1} and J_{Cutd} = −14.48 cm^{-1}, in agreement with the experimental values of −36.0(5) and −12.6(2) cm^{-1}, respectively. The B3LYP calculations lead to even worse results in model 3, where J_{tdtd} is close to zero (−1.8 cm^{-1}). It appears that the M06 functional performance for compound **2** is significantly better than that of B3LYP in calculating the intermolecular exchange coupling constants transmitted through $\pi-\pi$ contacts, leading to much more consistent results in models 2 and 3.

We have also performed calculations using model 4 in order to confirm our assumption that J_{CuCu} in compound **2** is weak and to test the behavior of J_{Cutd} in this simplified model that neglects next-nearest-neighbor (NNN) interactions (only two BS states). Indeed, $|J_{CuCu}|$ is smaller than 2 cm^{-1} regardless of the functional used, and the J_{Cutd} values are consistent with those obtained in models 1 and 3.

BS DFT Calculations for 3. BS DFT calculations for compound **3** were performed using four models comprising four different fragments of the crystal structure: a single [CuCl(td$^{\bullet-}$)$_2$]$^-$ complex anion as a three-spin model for the calculation of J_{Cutd1}, J_{Cutd2}, and J_{td1td2} (model 1, Figure S6a in the Supporting Information) and three two-spin models 2−4 for the calculations of the three different intermolecular J_{tdtd} coupling constants between td$^{\bullet-}$ radicals corresponding to three different $\pi-\pi$ contacts as depicted in Figure S6b−d, respectively). The results are summarized in Table 4 and Tables S14 and S15 in the Supporting Information. Both M06 and B3LYP calculations confirm antiferromagnetic interactions between Cu^{II} and the radical ligands with different J_{Cutd1} and J_{Cutd2} values. The next-nearest-neighbor-type (NNN) radical−radical interactions through the Cu^{II} centers is also antiferromagnetic but much weaker, ca. −4 cm^{-1}.

Table 4. Results of the BS DFT Calculations for Compound 3

model:	1			2	3	4
J/cm^{-1}	J_{Cutd2}	J_{Cutd1}	J_{td1td2}	J'_{tdtd}	J''_{tdtd}	J'''_{tdtd}
B3LYP	−22.59	−16.68	−4.37	+7.91	−22.56	−1.28
M06	−21.39	−15.71	−3.62	−19.97	−19.21	+0.83

The only significant difference between M06 and B3LYP calculated exchange coupling constants appears in model 2 (Figure S6b), where M06 predicts relatively strong antiferromagnetic interactions (−19.97 cm^{-1}) and B3LYP shows moderate ferromagnetic ones (+7.91 cm^{-1}). Since the fitting of the experimental data for **3** is not conclusive, it is difficult to choose the correct set of results. However, we assume that, similar to the BS DFT results for **2**, the M06 functional is also more reliable in the case of compound **3**.

The coupling constants, J_{tdtd}, calculated in model 3 (Figure S6c) are quite large (ca. −20 cm^{-1}); therefore, the related molecular $\pi-\pi$ contacts seem to be very efficient magnetic interaction pathways despite the large offset of the interacting radical anions. Calculations for model 4 demonstrate that the

https://dx.doi.org/10.1021/acs.inorgchem.0c01904
Inorg. Chem. 2020, 59, 13489−13501

magnetic interactions transmitted through the $\pi-\pi$-like contacts between the side C_5N rings of the phenanthroline backbone (Figure S6d) in compound **3** are negligible: −1.3 cm^{-1} in B3LYP and +0.8 cm^{-1} in M06.

These results support our assumption that compound **3** cannot be considered to be a magnetically isolated pair of $[CuCl(td^{\bullet-})_2]^-$ anions. Unfortunately, the difference between J_{Cutd2} and J_{Cutd1} interactions is not easily explained on the basis of the structural analysis. In Figure S3b, the spin density contours show no clear differences between the two ligands' arrangement in relation to the Cu^{II} localized spin density. Nonetheless, calculations support the difference in observed experimental coupling constants J_{Cutd2} and J_{Cutd1}.

Comment on BS DFT Calculations Using B3LYP vs M06 Functionals. The literature data agree that M06 performs similarly well to B3LYP when it comes to the BS DFT.[61,70] Indeed, our calculations of the magnetic interactions between Cu^{II} and the coordinated $td^{\bullet-}$ radical anions J_{Cutd} in compound **2** using B3LYP and M06 are similar and close to the experimental values regardless of the functional used. However, in the case of radical−radical magnetic interactions J_{tdtd} in compound **2**, the B3LYP functional gives values that are 2 times smaller than the experimental ones, while M06 reproduces them quite well. In our study, the only two cases in which B3LYP did not agree with M06 were the ones (models 2 and 3 for compound **2** and model 2 for compound **3**) in which one can point out $\pi-\pi$ interactions at a moderate distance covering the large contact surface of the molecules. A few other studies also highlight some advantages of using M06 for systems with intermolecular magnetic interactions.[71,72]

Electrochemistry. The electrochemistry of various Cu^{II}/Cu^{I} redox couples has been extensively studied in the past,[73−75] and has been shown to be strongly dependent on the coordination geometry. In particular, the impact of steric effects was noticed in copper complexes of 2,9-substituted-1,10-phenathrolines. However, compounds involving redox-active ligands are not very common.[4,76−80]

Cyclic voltammograms (CVs) for complexes **2** and **3** are presented in Figure 8 and Tables S17 and S18 as well as in Figure S7 in the Supporting Information. (Data for compound **1** was not collected due to very low solubility in MeCN.) CVs of **2** and **3** reveal three electrochemically reversible redox events in the −600 to −100 mV range vs Fc/Fc^+ and one (compound **3**) or two (compound **2**) electrochemically quasi-reversible/irreversible processes at lower potentials (below −800 mV). The three main processes (I−III; see Table 5 for the exact values of half potential $E_{1/2}$) are assigned in accordance with our findings related to the crystal structures of **2** and **3**.

ScXRD structural models showed that in compounds **2** and **3** $[Cu^{II}Cl(td^{\bullet-})(td)]$ and $[Cu^{II}Cl(td^{\bullet-})_2]^-$ are the respective stable states. Hence, the first two redox events, I and II, are most probably related to td ligands, while III is related to Cu^{II}/Cu^{I} couples which are slightly lower as compared to some literature reports for $[Cu^{II}(phen)_2]^+$ (phen = 1,10-phenanthroline derivatives)[73,74] (Scheme 1).

The three major redox processes (I−III) show very similar half potentials ($E_{1/2}$) in compound **2**, while in **3**, redox event III is shifted toward more negative values. The slight differences in the corresponding $E_{1/2}$ values for **2** and **3** might be ascribed to different starting geometries of the two complexes (Tables S4 and S19 in the Supporting Information). The splitting of $td/td^{\bullet-}$ into two separate events (I and II) is most probably due to the different coordination of the two ligands to the Cu center in both compounds. It is noteworthy that this difference is larger for compound **2**, leading to slightly stronger splitting of 135 mV as compared to that for **3** at 85 mV.

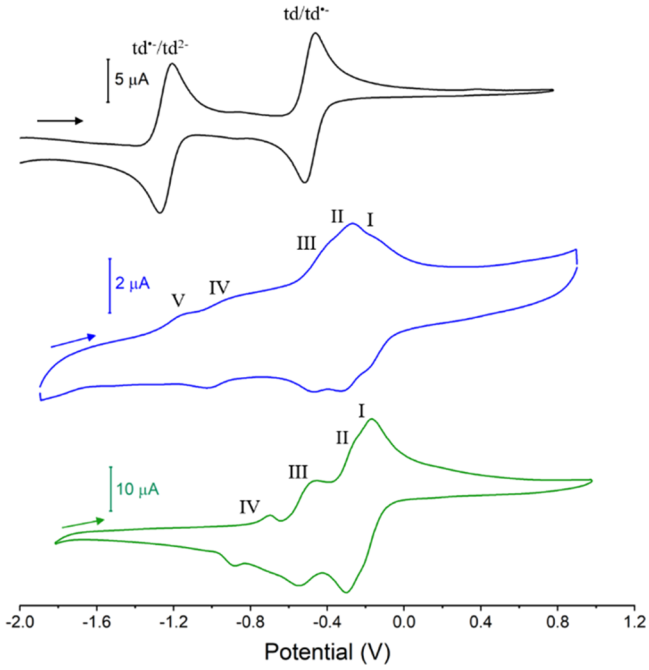

Figure 8. Cyclic voltammograms of a free td molecule (black), compound **2** (blue), and compound **3** (green) measured in 0.1 M $TBAPF_6$ solutions at a 200 mV/s scan rate vs Fc/Fc^+ (td at 100 mV/s). Arrows point in the direction of the potential sweep. Numbers assign peak pairs to redox events as presented in Scheme 1.

Table 5. Half-Potential Values for the Three Reversible Redox Processes in 2 and 3 (vs Fc/Fc^+)

	$E_{1/2}$ (ΔE_{pp})/mV	
redox process	2	3
I	−160 (60)	−196 (60)
II	−295 (58)	−281 (60)
III	−432 (64)	−514 (64)

Scheme 1. Assignment of the Redox Events in CVs of 2 and 3[a]

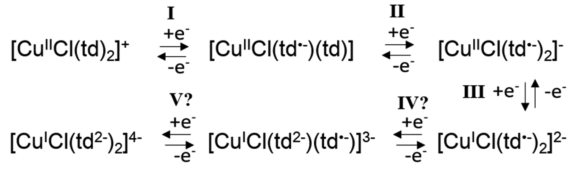

[a]The hypothetical assignments are marked with "?".

It is important to note that the reduction potential of [1,2,5]thiadiazolo[3,4-*f*][1,10]phenanthroline 1,1-dioxide in **2** and **3** is shifted by ca. 300 mV toward more positive values upon coordination to Cu^{II} (from −520 mV) as compared to the uncoordinated molecule. This is due to the electron-withdrawing properties of the positively charged metal ion.

Irreversible processes IV and V in **2** and **3** are most probably related to further reduction of the $td^{\bullet-}$ radical anions to their respective dianions. However, due to the high negative charge

https://dx.doi.org/10.1021/acs.inorgchem.0c01904
Inorg. Chem. 2020, 59, 13489−13501

of expected products $[Cu^{I}Cl(td^{2-})(td^{\cdot-})]^{3-}$ and $[Cu^{I}Cl(td^{2-})_2]^{4-}$, they might undergo a significant coordination geometry change, decomposition (ligand dissociation/substitution), or precipitation from the MeCN solution, resulting in the irreversible character of the corresponding electrochemical processes. These irreversible processes (IV and V), however, do not affect I, II, and III, as in the three consecutive CV cycles there are no signs of decomposition of **2** and **3** in MeCN (Figure S7 in the Supporting Information).

EXPERIMENTAL SECTION

Materials. All reagents were of analytical grade. CuCl (Alfa Aesar 97%) was recrystallized by the method described in ref 81 by diluting a concentrated hydrochloric acid solution with water. PPN(td)·$(CH_3)_2CO·H_2O$ was obtained according to a previously reported procedure.[56] [1,2,5]Thiadiazolo[3,4-*f*][1,10]phenanthroline 1,1-dioxide (td) was obtained according to the literature procedure.[54]

*Synthesis of {[CuCl(td)](μ-Cl)$_2$[CuCl(td)]} (**1**).* $CuCl_2·2H_2O$ (10.7 mg, 0.063 mmol) was dissolved in 10 mL of MeCN in a 50 mL vial. Then a test tube containing a suspension of 16.9 mg (0.063 mmol) of td filled to the edge was placed inside the vial. Finally, the 50 mL vial was gently filled with MeCN until the moment when the test tube contents and the vial solutions started to mix. This reaction setup was left undisturbed for 4 days, after which time green platelike crystals were collected and analyzed using PXRD. Yield: 99%. Anal. Calcd for {[CuCl(td)](μ-Cl)$_2$[CuCl(td)]}, $C_{24}H_{12}Cl_4Cu_2N_8O_4S_2$ (809.4 g/mol): C, 35.61; H, 1.49; N, 13.84. Found: C, 35.93; H, 1.66; N, 13.69.

*Synthesis of [CuCl(td$^{\cdot-}$)(td)]·2MeCN (**2**).* td (10.7 mg, 0.063 mmol) was refluxed in 55 mL of MeCN until most of it dissolved, and a solution of 39.6 mg (0.400 mmol) of CuCl in 5 mL of MeCN was added with stirring. After 1 min of stirring, the initial precipitate was filtered off while keeping the filtrate hot. The filtrate was sealed and left to crystallize at ca. 60 °C for 1 h. The dark-blue crystalline powder was collected, and its purity was confirmed by PXRD for a sample in contact with MeCN. Yield: 12.4 mg (18%). Anal. Calcd for $[CuCl(td^{\cdot-})(td)]·0.5H_2O$, $C_{24}H_{13}ClCuN_8O_{4.5}S_2$ (648.5 g/mol): C, 44.45; H, 2.02; N, 17.28. Found: C, 44.52; H, 2.10; N, 17.04. The samples of **2** undergo a very fast exchange of crystallized MeCN with water.

*Synthesis of PPN[CuCl(td$^{\cdot-}$)$_2$]·2DMA (**3**).* $CuCl_2·2H_2O$ (10.2 mg, 0.060 mmol) in 9 mL of DMA was added to a 9 mL DMA solution of 106.2 mg (0.120 mmol) of PPN(td)·$(CH_3)_2CO·H_2O$. The mixture was stirred for a few minutes, and then 90 mL of diethyl ether was layered on top of it. After ca. 20 h, small needlelike crystals were collected by filtration and washed with a small quantity of THF and diethyl ether. To obtain scXRD-quality crystals of **3**, a slow vapor diffusion method was used: 3 mL of the DMA mother solution prepared as described was transferred into a narrow vial which was then placed in a glass bottle with diethyl ether for 5 days. Large dark-violet needles were collected and used for the structure determination. The purity and identity of the bulk sample were checked by PXRD. Anal. Calcd for $PPN[CuCl(td^{\cdot-})_2]·1.5DMA·H_2O$, $C_{66}H_{57.5}ClCuN_{10.5}O_{6.5}P_2S_2$ (1326.8 g/mol): C, 59.75; H, 4.37; N, 11.08. Found: C, 59.73; H, 4.11; N, 11.01. The samples of **3** undergo a fast exchange of the crystallized DMA with water.

Physical Measurements. The single-crystal X-ray diffraction (scXRD) experiments were carried out using a Bruker D8 Quest Eco diffractometer equipped with a Photon 50 CMOS detector and a Mo Kα radiation source with a Triumph monochromator. Data were collected at 120(1) K using a Bruker Kryoflex II low-temperature device. Data integration and the absorption correction were performed using SAINT and SADABS or TWINABS (in the case of compound **1**) within the APEX3 suite of programs.[82] The space group determination was done using Xprep. The structure solution and refinement were carried out using SHELXT and SHELXL within the Olex2 graphical interface.[83] Hydrogen atoms were refined using the riding model, while all other atoms were refined anisotropically using weighted full-matrix least squares on F^2. Compound **1** was refined as a two-component twin.

Magnetic measurements were performed using a Quantum Design MPMS-3 Evercool SQUID magnetometer. The powder samples and a small quantity of the respective mother solutions were packed and sealed in double-layer high-density polyethylene foil bags to protect them from the loss of the crystallization solvent under vacuum. The data were corrected for the diamagnetism of the samples,[84] solvent, and foil. Fitting of the data was performed with PHI software.[68] Magnetic studies for compounds **1**−**3** dissolved in acetonitrile could not be performed due to their very limited solubility in MeCN.

Powder X-ray diffraction experiments were carried out using a Bruker D8 Advance Eco diffractometer equipped with a Cu Kα radiation source. The samples were ground under mother liquor to protect them from the solvent loss, and the respective suspensions were loaded into 0.5 or 0.7 mm glass capillaries.

Elemental analyses were carried out with an ELEMENTARY Vario Micro Cube CHNS analyzer.

Cyclic voltammetry was performed using an Mtm-anko M-161C electrochemical analyzer, a platinum working electrode, a platinum wire auxiliary electrode, and a silver wire as a pseudoreference. The potentials are given against an Fc/Fc^+ internal standard (Fc = ferrocene). The solvent of choice was MeCN, and the electrolyte was 0.1 M $TBAPF_6$ (tetrabutylammonium hexafluorophosphate). Compounds **2** and **3** were measured as saturated solutions. Compound **2** was found to be scarcely soluble, while the concentration of compound **3** was ca. 1.6 mM.

Computational Methodology. The magnetic interactions in **1**, **2**, and **3** were estimated using single-point broken symmetry (BS) density functional theory (DFT) following the Yamaguchi generalized projection scheme.[85−87] Unrestricted Kohn−Sham methods with B3LYP and M06 functionals were chosen.[88−91] All calculations were made in ORCA (versions 3.0.3, 4.1.1, and 4.2.1) with the RIJCOSX density fitting (also known as the resolution of identity, RI) approximation and a Def2-SVP-type auxiliary basis.[92,93] We have used Ahlrich's basis sets throughout this study.[94,95] Relatively small basis ma-Def2-SVP on C, H, N, and O atoms and Def2-TZVP on Cu, Cl, and S were selected to perform calculations presented in the main part of the article. A ORCA grid size of 6 was selected, and Douglas Kroll Hess (DKH) scalar relativistic corrections were applied for all of the calculations.[96] The basis set size dependence of the resulting exchange constants was estimated with a B3LYP functional only, using a simplified scheme that utilizes only two BS states for models 3 and 4. The results of these calculations are presented in Table S5 in the Supporting Information, with a suitable comment (Comment S1). The comparison between the results of RIJCOSX and no density fitting calculations (NORI) for compound **3** in model 2 showed no significant differences, thus approving the use of the RI approximation (Comment S2 and Table S16 in the Supporting Information). The structural fragments used for the calculations for compound **2** are schematically presented in Figure S4 in the Supporting Information. Coordinates for all structural models used in our calculations are taken from the .cif files. The reasoning behind their selection is described in section 2.5 of the main text.

Computations on model 4 of compound **2** were simplified to use only two BS states to save time. To do that, the assumption was made that the NNN and further magnetic contacts between spin carriers in model 4 are negligibly small. This is a relatively good approximation for that dimer because it presents good magnetic separation between other than the closest spin carriers. For model 2, however, we have used all five symmetrically relevant BS states. The spin density contours of the high-spin state models of compounds **1**−**3** calculated with the M06 functional are presented in Figures S3, S5, and S6 in the Supporting Information. Details on the derivation and computation of the exchange coupling constants from the DFT data can be found in Comments S3, S4, S5, S6, and S7 in the Supporting Information.

https://dx.doi.org/10.1021/acs.inorgchem.0c01904
Inorg. Chem. 2020, 59, 13489−13501

CONCLUSIONS

We have obtained and characterized three new coordination compounds utilizing a redox-active dioxothiadiazole, [1,2,5]-thiadiazolo[3,4-*f*][1,10]phenanthroline 1,1-dioxide (td), as a ligand: {[$Cu^{II}Cl(td)$](μ-$Cl)_2$[$Cu^{II}Cl(td)$]} (**1**), [$CuCl^{II}(td^{\cdot-})$-(td)]·2MeCN (**2**), and PPN[$Cu^{II}Cl(td^{\cdot-})_2$]·2DMA (**3**). These complexes are the first demonstrations of the coordination of the $td^{\cdot-}$ radical anion to a paramagnetic transition-metal ion. The function of the dioxothiadiazole ligand changes depending on its valence state. In its neutral diamagnetic form, it merely acts as a blocking ligand as demonstrated for compound **1**. In the anionic radical form, on the other hand, it takes control of the magnetic properties of compounds **2** and **3** and enables the construction of magnetically challenging systems. This is due to its strong tendency to form $\pi-\pi$ contacts which are very efficient magnetic interaction pathways as was demonstrated experimentally and by BS DFT theoretical calculations. Moreover, the experimental and theoretical investigations clearly show that the ligand is very useful for the construction of complex magnetic systems, and the reciprocal shift of the $td^{\cdot-}$ radicals can potentially reverse the sign of the magnetic coupling constants, leading to the observation of magnetic switching behavior.[55] Cyclic voltammetry revealed that in **2** and **3** the reduction of coordinated td ligands and Cu^{II} ions is within a very close range of potentials similar to the ones observed in guanidine- or dioxolene-based complexes exhibiting valence tautomerism.[21] These redox potentials should be sensitive to the geometry of the complex through simple td ligand modifications and through the exchange of the Cl^- anions.[73,74,97] Such modifications will lead to new catalysts,[98] light-harvesting complexes,[99,100] and magnetically switchable materials[21] taking advantage of the versatile and unique structural and redox properties of dioxothiadiazole molecules. Research in this vein is currently being pursued in our laboratory. Finally, comparison of the BS DFT calculations using B3LYP and M06 functionals for the reported systems leads to contradictory results when it comes to radical−radical magnetic interactions. It appears that only M06 results are in reasonably good agreement with the experiment. This questions the popular choice of the B3LYP functional for the BS DFT studies of radical−radical interactions with extensive delocalized π-orbital contact surfaces.

ASSOCIATED CONTENT

Supporting Information

The Supporting Information is available free of charge at https://pubs.acs.org/doi/10.1021/acs.inorgchem.0c01904.

Experimental PXRD patterns with Le Bail unit cell refinement results, additional structural diagrams, and computational details (PDF)

Accession Codes

CCDC 1998543−1998545 contain the supplementary crystallographic data for this paper. These data can be obtained free of charge via www.ccdc.cam.ac.uk/data_request/cif, or by emailing data_request@ccdc.cam.ac.uk, or by contacting The Cambridge Crystallographic Data Centre, 12 Union Road, Cambridge CB2 1EZ, UK; fax: +44 1223 336033.

AUTHOR INFORMATION

Corresponding Authors

Mirosław Arczyński − *Jagiellonian University, Faculty of Chemistry, 30-387 Kraków, Poland;* orcid.org/0000-0003-1948-9558; Email: miroslaw.arczynski@doctoral.uj.edu.pl

Dawid Pinkowicz − *Jagiellonian University, Faculty of Chemistry, 30-387 Kraków, Poland;* orcid.org/0000-0002-9958-3116; Email: dawid.pinkowicz@uj.edu.pl

Complete contact information is available at: https://pubs.acs.org/10.1021/acs.inorgchem.0c01904

Notes

The authors declare no competing financial interest.

ACKNOWLEDGMENTS

The authors gratefully acknowledge Dr. Veaceslav Vieru for fruitful discussions regarding the BS DFT calculations. This work was financed by the Polish National Science Centre within the Sonata Bis 6 project (2016/22/E/ST5/00055) and the Polish Ministry of Science and Higher Education within the "Diamond Grant" project (0041/DIA/2015/44). This research was supported in part by PLGrid Infrastructure.

REFERENCES

(1) Ferrando-Soria, J.; Vallejo, J.; Castellano, M.; Martínez-Lillo, J.; Pardo, E.; Cano, J.; Castro, I.; Lloret, F.; Ruiz-García, R.; Julve, M. Molecular Magnetism, Quo Vadis? A Historical Perspective from a Coordination Chemist Viewpoint. *Coord. Chem. Rev.* **2017**, *15*, 17−103.

(2) Urtizberea, A.; Natividad, E.; Alonso, P. J.; Pérez-Martínez, L.; Andrés, M. A.; Gascón, I.; Gimeno, I.; Luis, F.; Roubeau, O. Vanadyl Spin Qubit 2D Arrays and Their Integration on Superconducting Resonators. *Mater. Horiz.* **2020**, *7*, 885−897.

(3) Demir, S.; Jeon, I.-R.; Long, J. R.; Harris, T. D. Radical Ligand-Containing Single-Molecule Magnets. *Coord. Chem. Rev.* **2015**, *289*−*290*, 149−176.

(4) Himmel, H. J. Valence Tautomerism in Copper Coordination Chemistry. *Inorg. Chim. Acta* **2018**, *481*, 56−68.

(5) James, S. L.; Adams, C. J.; Bolm, C.; Braga, D.; Collier, P.; Friščic, T.; Grepioni, F.; Harris, K. D. M.; Hyett, G.; Jones, W.; et al. Playing with Organic Radicals as Building Blocks for Functional Molecular Materials. *Chem. Soc. Rev.* **2012**, *41* (1), 413−447.

(6) Drath, O.; Boskovic, C. Switchable Cobalt Coordination Polymers: Spin Crossover and Valence Tautomerism. *Coord. Chem. Rev.* **2018**, *375*, 256−266.

(7) Praneeth, V. K. K.; Ringenberg, M. R.; Ward, T. R. Redox-Active Ligands in Catalysis. *Angew. Chem., Int. Ed.* **2012**, *51* (41), 10228−10234.

(8) van der Vlugt, J. I. Radical-Type Reactivity and Catalysis by Single-Electron Transfer to or from Redox-Active Ligands. *Chem. - Eur. J.* **2019**, *25* (11), 2651−2662.

(9) Suarez, A. I. O.; Lyaskovskyy, V.; Reek, J. N. H.; Van Der Vlugt, J. I.; De Bruin, B. Complexes with Nitrogen-Centered Radical Ligands: Classification, Spectroscopic Features, Reactivity, and Catalytic Applications. *Angew. Chem., Int. Ed.* **2013**, *52* (48), 12510−12529.

(10) Ryu, Y.; Ahumada, G.; Bielawski, C. W. Redox- and Light-Switchable N-Heterocyclic Carbenes: A "Soup-to-Nuts" Course on Contemporary Structure−Activity Relationships. *Chem. Commun.* **2019**, *55* (31), 4451.

(11) Silavi, R.; Divsalar, A.; Saboury, A. A. A Short Review on the Structure-Function Relationship of Artificial Catecholase/Tyrosinase and Nuclease Activities of Cu-Complexes. *J. Biomol. Struct. Dyn.* **2012**, *30* (6), 752−772.

(12) Bryce, M. R. Recent Progress on Conducting Organic Charge-Transfer Salts. *Chem. Soc. Rev.* **1991**, *20* (3), 355−390.

(13) Fukuyama, H. Achievements and Challenges in Molecular Conductors. *Crystals* **2012**, *2* (3), 875−892.
(14) Uji, S.; Shinagawa, H.; Terashima, T.; Yakabe, T.; Terai, Y.; Tokumoto, M.; Kobayashi, A.; Tanaka, H.; Kobayashi, H. Magnetic-Field-Induced Superconductivity in a Two-Dimensional Organic Conductor. *Nature* **2001**, *410* (6831), 908−910.
(15) Lekin, K.; Ogata, K.; Maclean, A.; Mailman, A.; Winter, S. M.; Assoud, A.; Mito, M.; Tse, J. S.; Desgreniers, S.; Hirao, N.; et al. Pushing TC to 27.5 K in a Heavy Atom Radical Ferromagnet. *Chem. Commun.* **2016**, *52* (96), 13877−13880.
(16) Galán-Mascarós, J. R.; Coronado, E. Molecule-Based Ferromagnetic Conductors: Strategy and Design. *C. R. Chim.* **2008**, *11* (10), 1110−1116.
(17) Tamura, M.; Nakazawa, Y.; Shiomi, D.; Nozawa, K.; Hosokoshi, Y.; Ishikawa, M.; Takahashi, M.; Kinoshita, M. Bulk Ferromagnetism in the β-Phase Crystal of the p-Nitrophenyl Nitronyl Nitroxide Radical. *Chem. Phys. Lett.* **1991**, *186*, 401−404.
(18) Turek, P.; Nozawa, K.; Shiomi, D.; Awaga, K.; Inabe, T.; Maruyama, Y.; Kinoshita, M. Ferromagnetic Coupling in a New Phase of the P-Nitrophenyl Nitronyl Nitroxide Radical. *Chem. Phys. Lett.* **1991**, *180* (4), 327−331.
(19) Deumal, M.; Mota, F.; Bearpark, M. J.; Robb, M. A.; Novoa, J. J. Bulk Ferromagnetism in Nitronyl Nitroxide Crystals: A First Principles Bottom-up Comparative Study of Four Bulk Nitronyl Nitroxide Ferromagnets (KAXHAS, YOMYII, LICMIT and YUJNEW). *Mol. Phys.* **2006**, *104* (5−7), 857−873.
(20) Evangelio, E.; Ruiz-Molina, D. Valence Tautomerism: New Challenges for Electroactive Ligands. *Eur. J. Inorg. Chem.* **2005**, *2005*, 2957−2971.
(21) Himmel, H. J. Valence Tautomerism in Copper Coordination Chemistry. *Inorg. Chim. Acta* **2018**, *1*, 56−68.
(22) Tezgerevska, T.; Alley, K. G.; Boskovic, C. Valence Tautomerism in Metal Complexes: Stimulated and Reversible Intramolecular Electron Transfer between Metal Centers and Organic Ligands. *Coord. Chem. Rev.* **2014**, *268*, 23−40.
(23) Sato, O. Photoinduced Magnetization in Molecular Compounds. *J. Photochem. Photobiol., C* **2004**, *5* (3), 203−223.
(24) Phan, H.; Benjamin, S. M.; Steven, E.; Brooks, J. S.; Shatruk, M. Photomagnetic Response in Highly Conductive Iron(II) Spin-Crossover Complexes with TCNQ Radicals. *Angew. Chem., Int. Ed.* **2015**, *54* (3), 823−827.
(25) Zhang, J.; Matsushita, M. M.; Kong, X. X.; Abe, J.; Iyoda, T. Photoresponsive Coordination Assembly with a Versatile Logs-Stacking Channel Structure Based on Redox-Active Ligand and Cupric Ion [11]. *J. Am. Chem. Soc.* **2001**, *123* (48), 12105−12106.
(26) Sano, Y.; Tanaka, M.; Koga, N.; Matsuda, K.; Iwamura, H.; Rabu, P.; Drillon, M. Formation of Ferromagnetic Chains by Photolysis of 1:1 Complexes of Bis(Hexafluoroacetylacetonato)-Copper(II) with Diazodi-4-Pyridylmethane. *J. Am. Chem. Soc.* **1997**, *119* (35), 8246−8252.
(27) Naito, T.; Karasudani, T.; Mori, S.; Ohara, K.; Konishi, K.; Takano, T.; Takahashi, Y.; Inabe, T.; Nishihara, S.; Inoue, K. Molecular Photoconductor with Simultaneously Photocontrollable Localized Spins. *J. Am. Chem. Soc.* **2012**, *134* (45), 18656−18666.
(28) Drath, O.; Gable, R. W.; Moubaraki, B.; Murray, K. S.; Poneti, G.; Sorace, L.; Boskovic, C. Valence Tautomerism in One-Dimensional Coordination Polymers. *Inorg. Chem.* **2016**, *55* (9), 4141−4151.
(29) Guo, H.; Peng, Q.; Chen, X.-K.; Gu, Q.; Dong, S.; Evans, E. W.; Gillett, A. J.; Ai, X.; Zhang, M.; Credgington, D. High Stability and Luminescence Efficiency in Donor−Acceptor Neutral Radicals Not Following the Aufbau Principle. *Nat. Mater.* **2019**, *18* (September), 977.
(30) Hattori, Y.; Kimura, S.; Kusamoto, T.; Maeda, H.; Nishihara, H. Cation-Responsive Turn-on Fluorescence and Absence of Heavy Atom Effects of Pyridyl-Substituted Triarylmethyl Radicals. *Chem. Commun.* **2018**, *54* (6), 615−618.
(31) Wang, Y.; Jiang, Y.; Zhu, X.; Liu, M. Significantly Boosted and Inversed Circularly Polarized Luminescence from Photogenerated Radical Anions in Dipeptide Naphthalenediimide Assemblies. *J. Phys. Chem. Lett.* **2019**, *10* (19), 5861−5867.
(32) Pointillart, F.; Maury, O.; Le Gal, Y.; Golhen, S.; Cador, O.; Ouahab, L. 4-(2-Tetrathiafulvalenyl-Ethenyl)Pyridine (TTF-CH = CH-Py) Radical Cation Salts Containing Poly(β-Diketonate) Rare Earth Complexes: Synthesis, Crystal Structure, Photoluminescent and Magnetic Properties. *Inorg. Chem.* **2009**, *48* (15), 7421−7429.
(33) Jeon, I. R.; Park, J. G.; Xiao, D. J.; Harris, T. D. An Azophenine Radical-Bridged Fe2 Single-Molecule Magnet with Record Magnetic Exchange Coupling. *J. Am. Chem. Soc.* **2013**, *135* (45), 16845−16848.
(34) Zhang, W.-X.; Ishikawa, R.; Breedlove, B.; Yamashita, M. Single-Chain Magnets: Beyond the Glauber Model. *RSC Adv.* **2013**, *3* (12), 3772−3798.
(35) Degayner, J. A.; Wang, K.; Harris, T. D. A Ferric Semiquinoid Single-Chain Magnet via Thermally-Switchable Metal-Ligand Electron Transfer. *J. Am. Chem. Soc.* **2018**, *140* (21), 6550−6553.
(36) Clérac, R.; De, S.; Négrier, P.; Ma, X.; Dechambenoit, P.; Suturina, E. A.; Rouzières, M. A Redox-Active Bridging Ligand to Promote Spin Delocalization, High-Spin Complexes, and Magnetic Multi-Switchability. *Angew. Chem., Int. Ed.* **2018**, *57* (26), 7841−7845.
(37) Hicks, R. G. What's New in Stable Radical Chemistry? *Org. Biomol. Chem.* **2006**, *5* (9), 1321−1338.
(38) Ratera, I.; Veciana, J. Playing with Organic Radicals as Building Blocks for Functional Molecular Materials. *Chem. Soc. Rev.* **2012**, *41* (1), 303.
(39) Kaim, W.; Schwederski, B. Non-Innocent Ligands in Bioinorganic Chemistry-An Overview. *Coord. Chem. Rev.* **2010**, *254* (13−14), 1580−1588.
(40) Koivisto, B. D.; Hicks, R. G. The Magnetochemistry of Verdazyl Radical-Based Materials. *Coord. Chem. Rev.* **2005**, *249* (23), 2612−2630.
(41) Jobelius, H.; Wagner, N.; Schnakenburg, G.; Meyer, A. Verdazyls as Possible Building Blocks for Multifunctional Molecular Materials: A Case Study on 1,5-Diphenyl-3-(p-Iodophenyl)-Verdazyl Focusing on Magnetism, Electron Transfer and the Applicability of the Sonogashira-Hagihara Reaction. *Molecules* **2018**, *23* (7), 1758.
(42) Brook, D. J. R.; Fleming, C.; Chung, D.; Richardson, C.; Ponce, S.; Das, R.; Srikanth, H.; Heindl, R.; Noll, B. C. An Electron Transfer Driven Magnetic Switch: Ferromagnetic Exchange and Spin Delocalization in Iron Verdazyl Complexes. *Dalt. Trans.* **2018**, *47* (18), 6351−6360.
(43) Ovcharenko, V.; Romanenko, G.; Polushkin, A.; Letyagin, G.; Bogomyakov, A.; Fedin, M.; Maryunina, K.; Nishihara, S.; Inoue, K.; Petrova, M.; et al. Pressure-Controlled Migration of Paramagnetic Centers in a Heterospin Crystal. *Inorg. Chem.* **2019**, *58* (14), 9187−9194.
(44) Sun, J.; Sun, Z.; Wang, K.; Xi, L.; Ma, Y.; Li, L. Slow Relaxation of Magnetization in Unprecedented Cu−Ln-Rad Hetero-Tri-Spin Chains Constructed from Multidentate Nitronyl Nitroxide. *J. Mater. Chem. C* **2019**, *7* (29), 9057−9064.
(45) Jeon, I. R.; Negru, B.; Van Duyne, R. P.; Harris, T. D. A 2D Semiquinone Radical-Containing Microporous Magnet with Solvent-Induced Switching from Tc = 26 to 80 K. *J. Am. Chem. Soc.* **2015**, *137* (50), 15699−15702.
(46) Rupp, F.; Chevalier, K.; Graf, M.; Schmitz, M.; Kelm, H.; Grün, A.; Zimmer, M.; Gerhards, M.; van Wüllen, C.; Krüger, H. J.; et al. Spectroscopic, Structural, and Kinetic Investigation of the Ultrafast Spin Crossover in an Unusual Cobalt(II) Semiquinonate Radical Complex. *Chem. - Eur. J.* **2017**, *23* (9), 2119−2132.
(47) Zhou, B.; Ishibashi, S.; Ishii, T.; Sekine, T.; Takehara, R.; Miyagawa, K.; Kanoda, K.; Nishibori, E.; Kobayashi, A. Single-Component Molecular Conductor [Pt(Dmdt)2] - A Three-Dimensional Ambient-Pressure Molecular Dirac Electron System. *Chem. Commun.* **2019**, *55* (23), 3327−3330.
(48) Wang, H. Y.; Su, J.; Ma, J. P.; Yu, F.; Leong, C. F.; D'Alessandro, D. M.; Kurmoo, M.; Zuo, J. L. Concomitant Use of Tetrathiafulvalene and 7,7,8,8-Tetracyanoquinodimethane within the

https://dx.doi.org/10.1021/acs.inorgchem.0c01904
Inorg. Chem. 2020, 59, 13489−13501

Skeletons of Metal-Organic Frameworks: Structures, Magnetism, and Electrochemistry. *Inorg. Chem.* **2019**, *58*, 8657−8664.
(49) Manriquez, J. M.; Yee, G. T.; Mclean, R. S.; Epstein, A. J.; Miller, J. S. A Room-Temperature Molecular Organic Based Magnet. *Science (Washington, DC, U. S.)* **1991**, *252* (5011), 1415−1417.
(50) Pokhodnya, K. I.; Bonner, M.; Her, J. H.; Stephens, P. W.; Miller, J. S. Magnetic Ordering (Tc= 90 K) Observed for Layered [FeII(TCNE.-)(NCMe)2]+[FeIIICl4]-(TCNE = Tetracyanoethylene). *J. Am. Chem. Soc.* **2006**, *128* (49), 15592−15593.
(51) Kazakova, A. V.; Tiunova, A. V.; Korchagin, D. V.; Shilov, G. V.; Yagubskii, E. B.; Zverev, V. N.; Yang, S. C.; Lin, J. Y.; Lee, J. F.; Maximova, O. V.; et al. The First Conducting Spin-Crossover Compound Combining a MnIII Cation Complex with Electroactive TCNQ Demonstrating an Abrupt Spin Transition with a Hysteresis of 50 K. *Chem. - Eur. J.* **2019**, *25*, 10204−10213.
(52) Zhang, J.; Kosaka, W.; Kitagawa, Y.; Miyasaka, H. Host−Guest Hydrogen Bonding Varies the Charge-State Behavior of Magnetic Sponges. *Angew. Chem., Int. Ed.* **2019**, *58* (22), 7351−7356.
(53) Shuku, Y.; Awaga, K. Transition Metal Complexes and Radical Anion Salts of 1,10-Phenanthroline Derivatives Annulated with a 1,2,5-Tiadiazole and 1,2,5-Tiadiazole 1,1-Dioxide Moiety: Multidimensional Crystal Structures and Various Magnetic Properties. *Molecules* **2014**, *19* (1), 609−640.
(54) Shuku, Y.; Suizu, R.; Awaga, K. Monovalent and Mixed-Valent Potassium Salts of Thiadiazolo Phenanthroline 1, 1-Dioxide: A Radical Anion for Multidimensional Network Structures. *Inorg. Chem.* **2011**, *50*, 11859−11861.
(55) Shuku, Y.; Suizu, R.; Domingo, A.; Calzado, C. J.; Robert, V.; Awaga, K. Multidimensional Network Structures and Versatile Magnetic Properties of Intermolecular Compounds of a Radical-Anion Ligand, [1,2,5]Thiadiazolo[3,4- f][1,10]Phenanthroline 1,1-Dioxide. *Inorg. Chem.* **2013**, *52* (17), 9921−9930.
(56) Pakulski, P.; Arczyński, M.; Pinkowicz, D. Bis-(Triphenylphosphine)Iminium Salts of Dioxothiadiazole Radical Anions: Preparation, Crystal Structures, and Magnetic Properties. *Crystals* **2019**, *9* (1), 30.
(57) Mirífico, M. V.; Caram, J. A.; Gennaro, A. M.; Cobos, C. J.; Vasini, E. J. Radical Anions Containing the Dioxidated 1,2,5-Thiadiazole Heterocycle. Part II. *J. Phys. Org. Chem.* **2011**, *24* (11), 1039−1044.
(58) Linder, T.; Badiola, E.; Baumgartner, T.; Sutherland, T. C. Synthesis of π-Extended Thiadiazole (Oxides) and Their Electronic Properties. *Org. Lett.* **2010**, *12* (20), 4520−4523.
(59) Caram, J. A.; Jiménez Macías, J. P.; Arroyo, N. R.; Martínez Suárez, J. F.; Gennaro, A. M.; Echeverría, G. A.; Piro, O. E.; Mirífico, M. V. Stability of the Monoelectronic Reduction Product from 1,2,5-Thiadiazole S,S-Dioxides. Electrochemical, Chemical, and Photo-induced Doping. *ChemistrySelect* **2018**, *3* (30), 8729−8739.
(60) Pinkowicz, D.; Li, Z.; Pietrzyk, P.; Rams, M. New Thiadiazole Dioxide Bridging Ligand with a Stable Radical Form for the Construction of Magnetic Coordination Chains. *Cryst. Growth Des.* **2014**, *14* (10), 4878−4881.
(61) Valero, R.; Costa, R.; De, P. R.; Moreira, I.; Truhlar, D. G.; Illas, F. Performance of the M06 Family of Exchange-Correlation Functionals for Predicting Magnetic Coupling in Organic and Inorganic Molecules. *J. Chem. Phys.* **2008**, *128* (11), 114103.
(62) Blanchet-Boiteux, C.; Mouesca, J. M. End-on Azido-Bridged Copper Dimers: Spin Population Analysis and Spin Polarization Effect as Exhibited by Valence-Bond/Broken Symmetry, Density Functional Methods. *J. Am. Chem. Soc.* **2000**, *122* (5), 861−869.
(63) Onofrio, N.; Mouesca, J. M. Valence Bond/Broken Symmetry Analysis of the Exchange Coupling Constant in Copper(II) Dimers. Ferromagnetic Contribution Exalted through Combined Ligand Topology and (Singlet) Covalent-Ionic Mixing. *J. Phys. Chem. A* **2010**, *114* (20), 6149−6156.
(64) Castro, I.; Barros, W. P.; Calatayud, M. L.; Lloret, F.; Marino, N.; De Munno, G.; Stumpf, H. O.; Ruiz-García, R.; Julve, M. Dicopper(II) Pyrazolenophanes: Ligand Effects on Their Structures and Magnetic Properties. *Coord. Chem. Rev.* **2016**, *315*, 135−152.
(65) Ruiz, E.; Cano, J.; Alvarez, S.; Alemany, P. Broken Symmetry Approach to Calculation of Exchange Coupling Constants for Homobinuclear and Heterobinuclear Transition Metal Complexes. *J. Comput. Chem.* **1999**, *20* (13), 1391−1400.
(66) Kahn, O. Molecular Magnetism. *J. Chem. Educ.* **1995**, *72*, A19.
(67) Bauzá, A.; Mooibroek, T. J.; Frontera, A. The Bright Future of Unconventional σ/π-Hole Interactions. *ChemPhysChem* **2015**, *16* (12), 2496−2517.
(68) Kobylarczyk, J.; Pinkowicz, D.; Srebro-Hooper, M.; Hooper, J.; Podgajny, R. Anion-π Architectures of HAT(CN) 6 and 5d Polycyanidometalates: [W(CN) 8] 3-, [Re(CN) 7] 3-, and [Pt(CN) 6] 2-. *Cryst. Growth Des.* **2019**, *19* (2), 1215−1225.
(69) Chilton, N. F.; Anderson, R. P.; Turner, L. D.; Soncini, A.; Murray, K. S. PHI: A Powerful New Program for the Analysis of Anisotropic Monomeric and Exchange-Coupled Polynuclear d- and f-Block Complexes. *J. Comput. Chem.* **2013**, *34* (13), 1164−1175.
(70) Melo, J. I.; Phillips, J. J.; Peralta, J. E. Structural Dependence of Magnetic Exchange Coupling Parameters in Transition-Metal Complexes. *Chem. Phys. Lett.* **2013**, *557*, 110−113.
(71) Perić, M.; Zlatar, M.; Grubišić, S.; Gruden-Pavlović, M. Magnetic Couplings Mediated through the Non-Covalent Interactions. *Polyhedron* **2012**, *42* (1), 89−94.
(72) Singh, M. K.; Rajaraman, G. Can CH···π Interactions Be Used to Design Single-Chain Magnets? *Chem. - Eur. J.* **2015**, *21* (3), 980−983.
(73) Rorabacher, D. B. Electron Transfer by Copper Centers. *Chem. Rev.* **2004**, *104* (2), 651−698.
(74) Magni, M.; Colombo, A.; Dragonetti, C.; Mussini, P. Steric vs Electronic Effects and Solvent Coordination in the Electrochemistry of Phenanthroline-Based Copper Complexes. *Electrochim. Acta* **2014**, *141*, 324−330.
(75) Awad, D. J.; Conrad, F.; Koch, A.; Schilde, U.; Pöppl, A.; Strauch, P. 1,10-Phenanthroline-Dithiolate Mixed Ligand Transition Metal Complexes. Synthesis, Characterization and EPR Spectroscopy. *Inorg. Chim. Acta* **2010**, *363* (7), 1488−1494.
(76) Wiesner, S.; Wagner, A.; Kaifer, E.; Himmel, H. J. A Valence Tautomeric Dinuclear Copper Tetrakisguanidine Complex. *Chem. - Eur. J.* **2016**, *22* (30), 10438−10445.
(77) Oshio, H.; Yamamoto, M.; Ito, T. Cyanide-Bridged Molecular Squares with Ferromagnetically Coupled Dπ, Dσ, Pπ Spin System. *Inorg. Chem.* **2002**, *41* (22), 5817−5820.
(78) Devic, T.; Rondeau, D.; sahin, Y.; Levillain, E.; Clérac, R.; Batail, P.; Avarvari, N. Copper(I/II) Complexes of a Bis-(Tetrathiafulvalene)-2,2′-Bipyridine: Synthesis, Characterization, Magnetic and Electrochemical Properties. *Dalton Trans.* **2006**, 1331.
(79) Kahn, O.; Prins, R.; Reedijk, J.; Thompson, J. S. Orbital Symmetries and Magnetic Interaction between Copper(II) Ions and the o-Semiquinone Radical. Magnetic Studies of (Di-2-Pyridylamine)-(3,5-Di-Tert-Butyl-o -Semiquinonato)Copper(II) Perchlorate and Bis(Bis(3,5-Di- Tert-Butyl-o -Semiquinonato)Copper (II. *Inorg. Chem.* **1987**, *26* (21), 3557−3561.
(80) Luneau, D. Coordination Chemistry of Nitronyl Nitroxide Radicals Has Memory. *Eur. J. Inorg. Chem.* **2020**, *2020* (7), 597−604.
(81) Armarego, W. L. F.; Chai, C. *Purification of Laboratory Chemicals*, 7th ed.; Butterworth-Heinemann: Boston, 2013; Chapter 5, pp 555−661.
(82) *APEX2, SAINT, SADABS, Xprep*; Bruker AXS Inc.: Madison, WI, 2012.
(83) Dolomanov, O. V.; Bourhis, L. J.; Gildea, R. J.; Howard, J. A. K.; Puschmann, H. OLEX2: A Complete Structure Solution, Refinement and Analysis Program. *J. Appl. Crystallogr.* **2009**, *42* (2), 339−341.
(84) Bain, G.; Berry, J. F. Diamagnetic Corrections and Pascal's Constants. *J. Chem. Educ.* **2008**, *85* (4), 532−536.
(85) Shoji, M.; Koizumi, K.; Kitagawa, Y.; Kawakami, T.; Yamanaka, S.; Okumura, M.; Yamaguchi, K. A General Algorithm for Calculation of Heisenberg Exchange Integrals J in Multispin Systems. *Chem. Phys. Lett.* **2006**, *432* (1−3), 343−347.

https://dx.doi.org/10.1021/acs.inorgchem.0c01904
Inorg. Chem. 2020, 59, 13489−13501

(86) Shoji, M.; Koizumi, K.; Hamamoto, T.; Kitagawa, Y.; Yamanaka, S.; Okumura, M.; Yamaguchi, K. Hybrid-Density Functional Study of Magnetism and Ligand Control in Ni9 Complexes. *Chem. Phys. Lett.* **2006**, *421* (4−6), 483−487.
(87) Shoji, M.; Koizumi, K.; Kitagawa, Y.; Yamanaka, S.; Okumura, M.; Yamaguchi, K.; Ohki, Y.; Sunada, Y.; Honda, M.; Tatsumi, K. Theory of Chemical Bonds in Metalloenzymes V: Hybrid-DFT Studies of the Inorganic [8Fe−7S] Core. *Int. J. Quantum Chem.* **2006**, *106*, 3288−3302.
(88) Becke, A. Density Functional Thermochemistry III The Role of Exact Exchange. *J. Chem. Phys.* **1993**, *98*, 5648−5652.
(89) Lee, C.; Yang, W.; Parr, R. G. Development of the Colle-Salvetti Correlation-Energy Formula into a Functional of the Electron Density. *Phys. Rev. B: Condens. Matter Mater. Phys.* **1988**, *37* (2), 785−789.
(90) Zhao, Y.; Truhlar, D. G. Density Functionals with Broad Applicability in Chemistry. *Acc. Chem. Res.* **2008**, *41* (2), 157−167.
(91) Zhao, Y.; Truhlar, D. G. The M06 Suite of Density Functionals for Main Group Thermochemistry, Thermochemical Kinetics, Noncovalent Interactions, Excited States, and Transition Elements: Two New Functionals and Systematic Testing of Four M06-Class Functionals and 12 Other Function. *Theor. Chem. Acc.* **2008**, *120* (1−3), 215−241.
(92) Neese, F. The ORCA Program System. *Wiley Interdiscip. Rev.: Comput. Mol. Sci.* **2012**, *2* (1), 73−78.
(93) Neese, F. Software Update: The ORCA Program System, Version 4.0. *Wiley Interdiscip. Rev.: Comput. Mol. Sci.* **2018**, *8* (1), 4−9.
(94) Weigend, F.; Ahlrichs, R. Balanced Basis Sets of Split Valence, Triple Zeta Valence and Quadruple Zeta Valence Quality for H to Rn: Design and Assessment of Accuracy. *Phys. Chem. Chem. Phys.* **2005**, *7* (18), 3297−3305.
(95) Weigend, F. Accurate Coulomb-Fitting Basis Sets for H to Rn. *Phys. Chem. Chem. Phys.* **2006**, *8* (9), 1057−1065.
(96) Douglas, M.; Kroll, N. M. Quantum Electrodynamical Corrections to the Fine Structure of Helium. *Ann. Phys. (Amsterdam, Neth.)* **1974**, *82* (1), 89−155.
(97) Crispini, A.; Cretu, C.; Aparaschivei, D.; Andelescu, A. A.; Sasca, V.; Badea, V.; Aiello, I.; Szerb, E. I.; Costisor, O. Influence of the Counterion on the Geometry of Cu(I) and Cu(II) Complexes with 1,10-Phenanthroline. *Inorg. Chim. Acta* **2018**, *470*, 342−351.
(98) Huang, Z.; Askari, M. S.; Esguerra, K. V. N.; Dai, T. Y.; Kwon, O.; Ottenwaelder, X.; Lumb, J. P. A Bio-Inspired Synthesis of Oxindoles by Catalytic Aerobic Dual C-H Functionalization of Phenols. *Chem. Sci.* **2016**, *7* (1), 358−369.
(99) Hattori, S.; Wada, Y.; Yanagida, S.; Fukuzumi, S. Blue Copper Model Complexes with Distorted Tetragonal Geometry Acting as Effective Electron-Transfer Mediators in Dye-Sensitized Solar Cells. *J. Am. Chem. Soc.* **2005**, *127* (26), 9648−9654.
(100) Ashbrook, L. N.; Elliott, C. M. Dye-Sensitized Solar Cell Studies of a Donor-Appended Bis(2,9-Dimethyl-1, 10-Phenanthroline) Cu(I) Dye Paired with a Cobalt-Based Mediator. *J. Phys. Chem. C* **2013**, *117* (8), 3853−3864.

https://dx.doi.org/10.1021/acs.inorgchem.0c01904
Inorg. Chem. 2020, 59, 13489−13501